J. At. Mol. Sci.
doi: 10.4208/jams.102711.112911a

Vol. **3**, No. 4, pp. 344-352
November 2012

Tuning of plasmon resonance through gold slit arrays with Y-shaped channels

Jin- Jun Wu[a], Hong-Jian Li[a,b*], Yong Zeng[a], Xiao Peng[a], Zhi-Min Liu[a], and Guang-Tao Cao[b]

[a] *College of Physics Science and Technology, Central South University, Changsha 410083, China*
[b] *College of Materials Science and Engineering, Central South University, Changsha 410083, China*

Received 27 October 2011; Accepted (in revised version) 29 November 2011
Published Online 18 May 2012

Abstract. We propose gold slit arrays with Y-shaped channels and investigate their transmission properties numacially. Results indicate that the surface plasmon resonance peak value keeps unchanged and the localized waveguide resonance peak red-shifts and falls obviously when the entrance slit width narrows. However when the entrance slit becomes extremely small the surface plasmon resonance peak red-shifts and falls sharply. Furthermore as the slit length increases, firstly the surface plasmon resonance peak splits into two peaks, the right peak value rise and they slowly converged into one single peak. To understand its physical origin, surface plasmon resonance and Fabry-Perot cavity resonance theories are suggested. We simulate their electric field distributions and find the electric fields become stronger as the slit become narrower or the dielectric constant become smaller. The results may be useful for the design of frequency-selective sensor and optical devices in the future.

PACS: 73.20.Mf, 78.20.-e, 78.67.-n

Key words: Y-shape channel slit array, optical transmission, surface plasmon resonance, localized waveguide resonance

1 Introduction

Extraordinary optical transmission(EOT) through sub-wavelength hole array perforated on metal film has inspired great interest since it was first reported by Ebbesen etc[1]. Besides of sub-wavelength hole arrays [2,3], slit and slit array[4-7] are topics of considerable fascination to achieve extraordinary high transmission in several applications [8-10],

*Corresponding author. *Email address:* : lihj398@yahoo.com.cn (H. J. Li)

including super-lenses, optical filters and microscopy. The initial work owes EOT to surface plasmon, but surface plasmon is not the sole factor contributing to EOT, it even has a negative influence in some case, like one-dimension metallic gratings [6]. Attention of EOT is mostly focused on the study of the influence of the shape, size, and periodicity of the metallic hole or slit array with straight channels [11,12]. Recently, notice has been taken of a hole or slit with a shaped channel, including a hole array with converging-diverging shaped channels [13-15], and a single slit with a stepped channel [16]. A slit or hole with a bent channel has also been researched [17,18]. Investigations of the bent channel metallic structure are mostly concentrated on the transmission of the structure as a single waveguide. Transmission properties of the periodic slit or hole arrays with bent channels [19] have been scarcely studied up to now. So this paper designs gold slit arrays with Y-shaped channels and investigate its transmission properties numacially.

In this paper, we investigate the transmission properties of the gold slit array with Y-shaped channel by employing the two-dimensional (2D) finite-difference time-domain (FDTD) method. The influence of the bent slit geometry parameters on the transmission spectrum has been discussed in detail. The results obtained here are helpful to design new sub-wavelength optical devices.

2 Model and simulation method

The analyzed structure is presented in Fig. 1. In our 2D FDTD calculations [20], perfectly matched layer boundary conditions [21] are used 2250 nm away from the interfaces of the gold film in the z and -z directions. And periodic boundary conditions are used above and below the slit due to the periodicity of the structure. We simulate the structure with a computational window of $L_y \times L_z = 750$ nm $\times$ 5250 nm, where the structure in the x direction is uniform and infinite. The structure is periodic in the y direction, and the period is $p = 750$ nm. The spatial and temporal steps are set as $\Delta y = \Delta z = 3.5$ nm and (c is the velocity of light in vacuum), and we send a Gaussian single pulse of light with a wide frequency profile. The probe location is set at away from the rear surface of the gold film, and the transmission spectrum is normalized by the calculation without a metallic structure.

The incident light impinges on the structure in the z direction with a polarization along the y direction. A schematic view in the y-z cross section of a lattice of the bent slit array in a freestanding gold film is shown in Fig. 1. The frequency-dependent permittivity of the metal is described by the Drude model:

$$\varepsilon = 1 - \frac{\omega_p^2}{\omega^2 + \gamma^2} + i\frac{\omega_p^2 \gamma}{\omega(\gamma^2 + \omega^2)} \tag{1}$$

where ω_p is the plasma frequency, γ is the collision frequency related to energy loss, and ω stands for the frequency. The parameters used in the Drude model for Au are $\omega_p = 1.374 \times 10^{16} \mathrm{s}^{-1}$ and $\gamma = 4.08 \times 10^{13} \mathrm{s}^{-1}$.

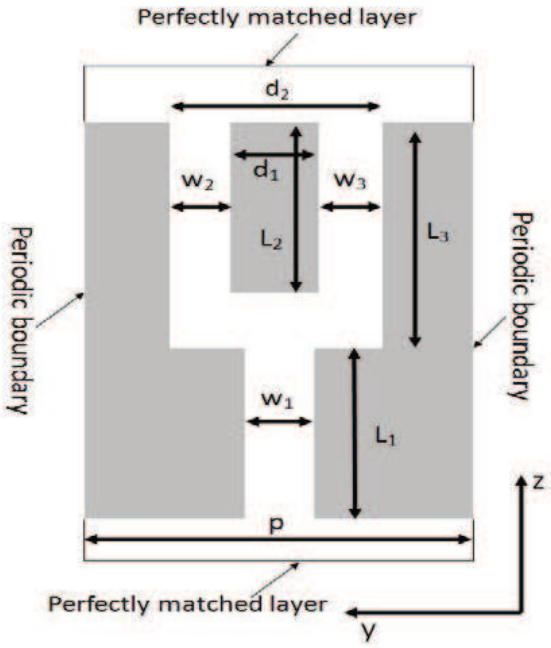

Figure 1: Scheme of a unit cell of the gold film perforated with Y-shaped channels.

3 Results and discussion

In this section, we numacially study the resonance properties of the gold bent slit array. In the whole paper, the period p and incident angle θ of the bent slit array are kept constant as 750 nm and 0° respectively. The slit widths w_1, w_2, w_3, d_2, metal width and slit lengths L_1, L_2, L_3 are used as tuning parameters.The original parameters are set as $w_1 = w_2 = w_3 =$ 150 nm, $L_1 = 150$ nm, $L_2 = 350$ nm, $L_3 = 500$ nm, $d_1 = 200$ nm, $d_2 = 500$ nm.

Firstly we investigate the transmission behaviors of the metal arrays with different geometry structure parameters. For example we change the entrance slit width w_1 while other parameters are fixed. It can be found that when $\lambda = 0.764 * aa$(aa is the lattice constant), namely λ is about the period length of the structure, its transmission rate is zero, this phenomenon is called wood abnormity. As reported in Ref. [23], the shorter wavelength transmission resonance peak is mostly associated with the surface plasmon resonance, and the longer wavelength peak is relative to the localized waveguide resonance for the periodic metal hole array with straight channel. From Fig. 2(a), we can see the value and position of surface plasmon resonance peak keep unchanged when the slit width w_1 decreases from 300 nm to 50 nm, but its full width at half maximum becomes narrow. This property can be used to design frequency-selective device to filter narrower bandwidth light, however when w_1 becomes extremely small, the peak of surface plasmon resonance falls sharply and red-shift swiftly.

According to Ref. [24, 25], the surface plasmon resonance mode would red-shift slightly with the decrease of slit width, However, in our simulation the magnitude and position of surface plasmon resonance almost keep the same when the slit width w_1 decreases in some range. It may be explained that as slit width w_1 decreases, a resonance cavity forms in the middle section of the Y-shaped slit, and the light in it reflect and intensify constantly, which counteracts the energy loss in the left sections of the slit.

On the other hand, the localized waveguide resonance red-shifts and decreases manifestly when the width w_1 becomes very small, for example, when the slit width decreases from 300 nm to 200 nm or from 200 nm to 100 nm, the resonance peak red-shifts 0.172 nm and 0.236 nm respectively, and the resonance peak value decreases 0.1594 and 0.4307, respectly.

The localized waveguide resonance mode is characterized by constructive interference along the channel between all partial transmitted waves, in the way of the Fabry-Perot cavity mode [26]. The Fabry-Perot condition can be expressed as follows [27]:

$$K_0 Re(n_{eff})l + \arg(\rho) = n\pi \tag{2}$$

where *rho* the reflection coefficient of this fundamental mode and n is a signed integer. n_{eff} is the effective refractive index of the fundamental Bloch mode propagating in the slit, and l is the slit length. It is demonstrated that the narrower the slit, the stronger the coupling between the charge densities of the two walls, and the effective refractive index increases quickly with the decrease of the slit width especially when the slit width is very small [28]. If n is a constant, larger n_{eff} needs smaller k_0 or larger wavelength to meet the Fabry-Perot condition, so the localized waveguide resonance mode will red-shift when the slit becomes narrower and the mode will red-shift more distinctly when the width w_1 is extremely small.

Also we study the transmission behaviors for different exit slit widths w_2 and w_3

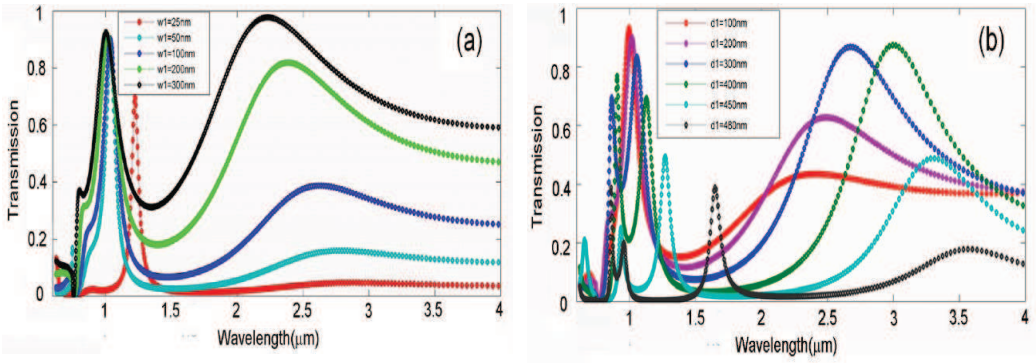

(a) (b)

Figure 2: Transmission spectra of the gold film perforated with Y-shaped channels as a function of wavelength for different entrance slit widths(a) and exit slit widths(b).

shown in Fig. 2(b). As the metal width d_1 increases, the exit slit widths w_2 and w_3 decrease. We find that surface plasmon resonance mode red-shifts and decreases swiftly when the exit slit width decrease from 200 nm to 100 nm, but when the exit slit width is smaller than 100 nm, the surface plasmon resonance mode splits and there are many new resonance modes in shorter wavelength. It is worthy to note that a very broad wavelength band gap range from 1000 nm to 1500 nm appears when $d_1 = 480$ nm (black line). light in this wavelength range can not transmit through the structure. The results can be applied to design an optical filter or frequency selector in this wavelength range.

The wavelength that corresponds to an in-plane surface plasmon resonance [29] can be expressed as

$$\lambda = \frac{p}{\sqrt{i^2+j^2}}\sqrt{\frac{\varepsilon_d\varepsilon_m}{\varepsilon_d+\varepsilon_m}} \tag{3}$$

where p is the grating period, i and j are integers, ε_d and ε_m are the relative dielectric constants of metal and dielectric respectivelyand $\sqrt{\frac{\varepsilon_d\varepsilon_m}{\varepsilon_d+\varepsilon_m}}$ is the effective refractive index. As the slit width decreases, effective refractive index of the structure increases, so λ becomes larger, which means the surface plasmon resonance mode red-shifts, and when the effective refractive index of the structure is larger than a certain value, i and j can have many larger values to satisfy Eq. (3), so the surface plasmon resonance mode splits and many new resonance modes appear in shorter wavelength.

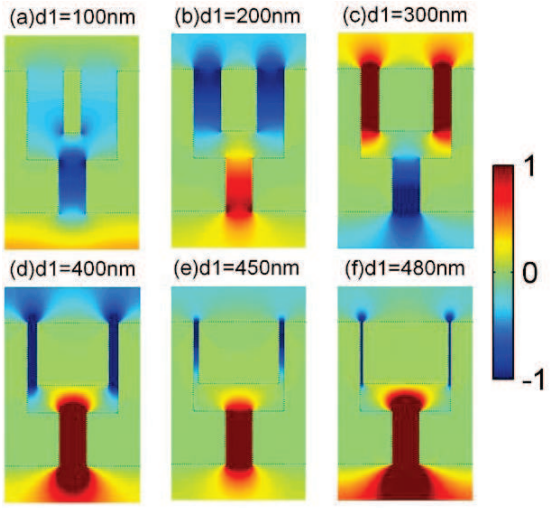

Figure 3: The spatial distribution of the electronic field component Ex of the model for different exit slit widths.

Also as the exit slit width decreases, the localized waveguide resonance mode red-shifts obviously, its explanation is similar to that of w_1 . What interests me is that firstly the localized waveguide resonance peak rises, and then keeps stable, finally it falls sharply. In order to shoot light on its physical mechanics, we simulate the electronic field spatial

distribution corresponding to the localized waveguide resonant peak. On the one hand, the narrower the exit slit, the stronger the coupling between the charge densities of the two walls, and the stronger the magnitude of the electronic field. So the localized waveguide resonance peak risesbut on the other hand , when the exit slit becomes narrower, it restrains the amount of light shoot out, so in a certain scope, the two opposite factors counteract with each other and the localized waveguide resonance peak keeps stable. But when the exit slit becomes extremely narrow, the restrain effect plays a predominant role in the transmission and the peak falls sharply, at this time the electronic field is mainly distributed in the entrance slit shown in Fig. 3. Areas colored red represents positive field amplitude, while areas colored blue means negative field amplitude

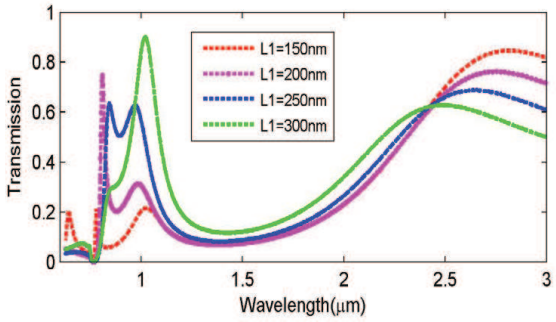

Figure 4: Transmission spectrum of the gold film perforated with Y-shaped channels as a function of wavelength for different slit lengths L_1.

Also we investigate the transmission property with different entrance slit lengths shown in Fig. 4 . As the slit length L_1 increases, firstly the surface plasmon resonance peak splits into two peaks, the right peak value rise and they slowly converged into one single peak. When slit length increases, it is equivalent that the slit width narrows, then the effective refractive index increase. According to Eq. (2), the equation meets at the longer wavelength. Considering thicker metal films, there is a critical width for which the equation is satisfied at two different wavelengths with different i and j, correspondingly, the surface plasmon resonance peak splits into two peaks, and when the slit length L_1 continues to increase, there is only one wavelength that can meet Eq. (2), so the two peaks slowly converged into one single peak.

Next the transmission property of the structure with different stuffing dielectrics in the slit is also investigated as shown in Fig. 5. It is obvious that with the increase of the dielectric constants of the stuffing dielectrics, the surface plasmon resonance peak slowly red-shifts and falls, also several new high order resonance modes appear in shorter wavelength and the localized waveguide resonance mode red-shifts more quickly than the surface plasmon resonance mode .but its peak value keeps the same.

With the increase of the dielectric constant, the free electrons in the dielectrics decrease, this leads to the decrease of the surface plasmon in the interface of the mental and the dielectrics and the near field enhancement effect caused by the surface plasmon reso-

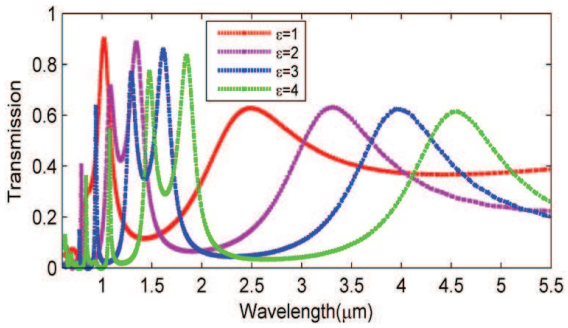

Figure 5: Transmission spectrum of the gold film with Y-shaped channels as a function of wavelength for different stuffing dielectrics.

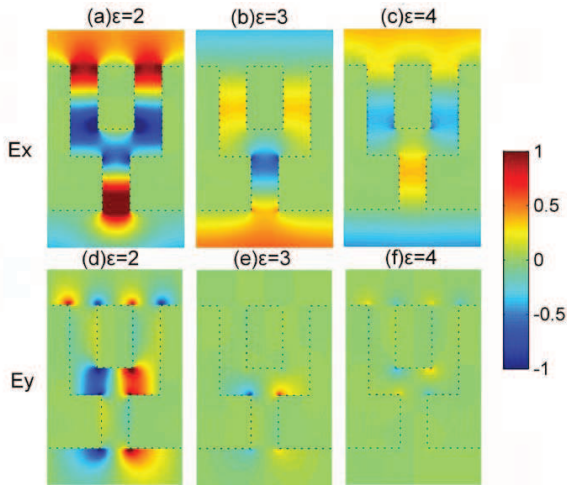

Figure 6: The spatial distribution of electronic field of the model for different dielectric constants.

nance became weaker, which finally results in the fall of the surface plasmon peak. This can be proved by the electronic field distribution of the structure with different dielectric constants shown in Fig. 6. It can be found that as the dielectric constant become larger, the electric field actually become weaker.

Areas colored red represents positive field amplitude, while areas colored blue means negative field amplitude. We can see coupled standing wave patterns inside each slit formed along the longitudinal direction from the field distribution of $|E_x|$ in Fig. 6. Second, the calculated results of the electric field E_y distribution in Fig. 6 indicate an alternation of positive and negative values of E_y near the edges of the slit along the x-direction, which means that the oscillation of the charge density exists. In other words, these pictures indicated that the SP wave really exists and the SP propagating along the grating surface. We can see that the sign of E_y value for each slit at the entrance is the same as that

at the exit along z direction, while it is opposite for two sides of the entrance or exit. From the view of the whole grating, we also can consider that there exist dipole, quadrupole, hexapole and multipole plasmon mode.

According to Eq. (2), as the relative dielectric constant of metal ε_d increases, the effective refractive index $n_{eff}\sqrt{\frac{\varepsilon_d\varepsilon_m}{\varepsilon_d+\varepsilon_m}}$ increases. When n keeps constant, as ε_d become larger, $k_0=\frac{2\pi}{\lambda}$ must be smaller or λ larger to meet the equation ,so the peak of localized waveguide resonance red-shifts.

4 Conclusions

We propose sub-wavelength mental arrays with Y-shaped channels and simulate their transmission property by using finite-difference time-domain (FDTD) methods. The influences of the slit geometry parameters on the transmission spectrum have been investigated in detail. We finf that the surface plasmon resonance peak value keeps unchanged and the localized waveguide resonance peak red-shifts and falls obviously when the entrance slit width narrows, however when the entrance slit becomes extremely small the surface plasmon resonance peak red-shifts and falls sharply. Furthermore as the slit length increases, firstly the surface plasmon resonance peak splits into two peaks, then the right peak value rise and they slowly converged into one single peak. To understand its physical mechanism, surface plasmon resonance and Fabry-Perot cavity resonance theories are suggested. We simulate their electric field spatial distributions and find the electric fields become stronger as the slit become narrower or the dielectric constant become smaller.These properties may be helpful for the design of new optical device.

Acknowledgments This work was funded by the Research Fund for the Doctoral Program of Higher Education of China under Grant No. 20100162110068 and the National Natural Science Foundation of China under Grant No. 11164007.

References

[1] T. W. Ebbesen, H. F. Ghaemi, T. Thio, *et al.*, Nature, 391 (1998) 667.
[2] J. Dintinger, S. Klein, F. Bustos, W. L. Barnes, *et al.*, Phys. Rev. B 71 (2005) 035424.
[3] W. L. Barnes, W. A. Murray, J. Dintinger, *et al.*, Phys.Rev. Lett. 92 (2004) 107401.
[4] S. Astilean, P. Lalanne, and M. Palamaru, Opt. Commun. 175 (2000)165.
[5] Y. Takakura, Phys. Rev. Lett. 86 (2001) 5601.
[6] Q. Cao and P. Lalanne, Phys. Rev. Lett. 88 (2002) 057403.
[7] Y. Xie, A. Zakharian, J. Moloney, and M. Mansuripur, Opt. Express 13 (2005) 4485.
[8] Z. Sun and H. K. Kim, Appl. Phys. Lett. 85 (2004) 642
[9] M. W. Docter, I. T. Young, O. M. Piciu, *et al.*, Opt. Express 14 (2006) 9477.
[10] M. H. Chowdhury, J. M. Catchmark, and J. R. Lakowicza, Appl. Phys. Lett. 91 (2007) 103118.
[11] Y. Xie, A. R. Zakharian, J. V. Moloney, *et al.*, Opt. Express 13(2005) 4485.
[12] Y. Xie, A. R. Zakharian, J. V. Moloney, *et al.*, Opt. Express 14(2006)10220.

[13] A. Battula and S. C. Chen, Appl. Phys. Lett. 89 (2006) 131113.
[14] A. Battula, Y. L. Lu, R. J. Knize, *et al.*, Opt. Express 15 (2007) 14629.
[15] W. Wang, Y. L. Lu, R. J. Knize, *et al.*, Opt. Express 17 (2009)7361.
[16] M. J. Lockyear, A. P. Hibbins, and J. R. Sambles, Appl. Phys. Lett. 91 (2007) 251106.
[17] D. R. Mason, D. K. Gramotnev, and K. S. Kim, Opt. Express 18 (2010) 16139.
[18] T. W. Lee and S. K. Gray, Opt. Express 13 (2005) 9652.
[19] S. X. Xie, H. J. Li, X. Zhou, *et al.*, J. Opt. Soc. Am. A 28 (2011) 441.
[20] A. Taflove and S. C. Hagness, Computational Electrodynamics: The Finite-Difference Time-Domain Method (Artech, 2005).
[21] J. P. Berenger, J. Comput. Phys. 114 (1994) 185.
[22] M. A. Ordal, L. L. Long, R. J. Bell, *et al.*, Appl. Opt. Express 22 (1983) 1099.
[23] Z. C. Ruan and M. Qiu, Phys. Rev. Lett. 96 (2006) 233901.
[24] H. Shi, C. Wang, C. Du, Opt. Express, 13 (2005) 6815.
[25] Y. Pang, C. Genet, and T. W. Ebbesen, Opt. Commun. 280 (2007)10.
[26] A. P. Hibbins, M. J. Lockyear, J. R. Sambles, J. Appl. Phys. 99 (2006) 124903.
[27] C. Sauvan, J. P. Hugonin, J. C. Rodier, *et al.*, Phys. Rev. B 68 (2003) 125404.
[28] H. Shi, C. Wang, C. Du, *et al.*, Opt. Express 13 (2005) 6815.
[29] J. E. Kihm and Y. C. Yoon, Phys. Rev. B 75 (2007) 035414.